

Article

One-Pot Synthesis of 2,5-Diformylfuran from Fructose by Bifunctional Polyaniline-Supported Heteropolyacid Hybrid Catalysts

Shuqing Liu, Xing Fu, Jinhang Dai, Zhongbao Liu, Liangfang Zhu * and Changwei Hu *

Key Laboratory of Green Chemistry and Technology Ministry of Education, College of Chemistry, Sichuan University, Chengdu, Sichuan 610064, China; liushuqing93@163.com (S.L.); fuxing1804@163.com (X.F.); jinhang.dai@foxmail.com (J.D.); authenticscu@live.cn (Z.L.)

* Correspondence: zhulf@scu.edu.cn (L.Z.); changwei@scu.edu.cn (C.H.); Tel.: +86-28-8541-5608 (L.Z.); +86-28-85411105 (C.H.)

Received: 12 April 2019; Accepted: 10 May 2019; Published: 13 May 2019



Abstract: We report the preparation of bifunctional hybrid catalysts by supporting $\text{H}_3\text{PMo}_{12}\text{O}_{40}$ (PMo_{12}) heteropolyacid (HPA) on polyaniline (PAN) or formyl-functionalized PAN (F-PAN) for the “one-pot” and “one-step” synthesis of 2,5-diformylfuran (DFF) from fructose via 5-hydroxymethylfurfural (HMF) intermediate. We show that the PMo_{12} HPA is the main active species for both fructose dehydration and HMF oxidation owing to its Brønsted acidic and redox characters. However, the anchoring of PMo_{12} on PAN reduces the Brønsted acidity by acid–base interaction between protons in HPA and quinoid diimine structure in PAN, thereby reducing the dehydration performance. We demonstrate that the catalytic dehydration performance of the hybrid catalyst could be strengthened by grafting formyl groups on PAN before HPA anchoring. The highest DFF yield of 76.7% is obtained by conducting the “one-pot” reaction over the 40- PMo_{12} /F₃-PAN catalyst at 413 K for 7 h in air, wherein the side-reactions of fructose or HMF degradation and HMF rehydration have been significantly reduced. This hybrid catalyst is reusable without significant activity loss, highlighting the designing of stable inorganic–organic hybrid catalysts for producing valuable hexose-derived platform chemicals.

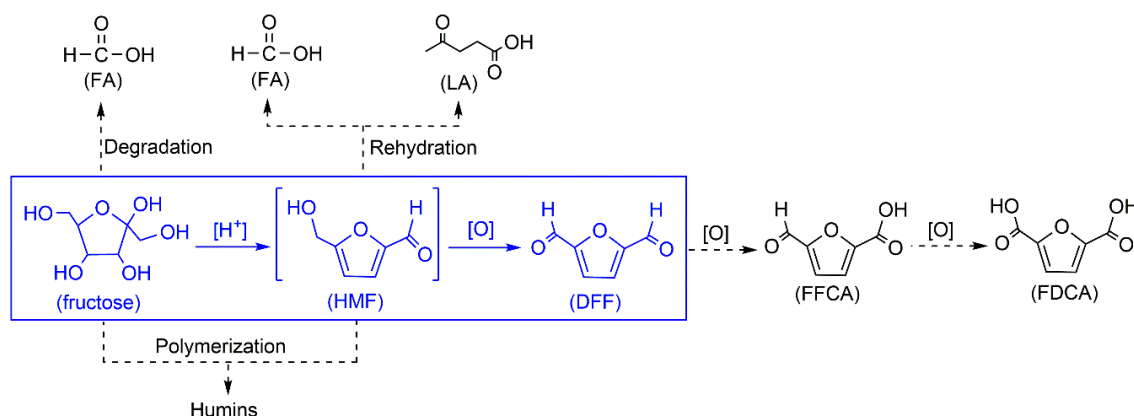
Keywords: 2,5-diformylfuran; one-pot reaction; bifunctional catalysis; inorganic-organic hybrid catalysts; polyaniline

1. Introduction

The abundant and renewable biomass resource has been regarded as an ideal alternative to replace non-renewable fossil resources for producing value-added fine chemicals and liquid fuels [1]. So far, various value-added chemicals have been produced from cellulosic biomass [2–5]. Among others, 2,5-diformylfuran (DFF), the partially oxidized product from 5-hydroxymethylfurfural (HMF), is considered as one of the most promising platform molecules owing to its broad potential as an intermediate for pharmaceuticals, fungicides, macrocyclic ligands, and as a cross-linker or monomer for novel polymeric materials [6,7]. Despite the high DFF yields (>90%) from the aerobic oxidation of pure HMF [8–18], the direct synthesis of DFF from fructose via HMF as an intermediate is more attractive since the separation and purification of HMF is energy-intensive because of the unstable characteristic of HMF during the acid-catalyzed HMF production. Nowadays, the development of a facile and highly selective “one-pot” strategy for fructose-to-DFF conversion is challenging.

Fructose-to-DFF conversion is a tandem reaction involving fructose-to-HMF dehydration over acid sites and subsequent HMF-to-DFF oxidation over redox sites (Scheme 1). However, the water formed during the foregoing dehydration step decelerates the following oxidation step.

Furthermore, the co-existence of acid sites, redox sites, and water in the catalytic system always leads to the generation of a large amount of by-products (i.e., formic acid (FA), levulinic acid (LA), and humins) from the oxidative-degradation/polymerization of fructose and rehydration/polymerization of HMF. Therefore, a popular “one-pot” and “two-step” method has been developed for fructose-to-DFF conversion, wherein the acid and redox catalysts were added stepwise, giving out high DFF yields ranging from 70% to 80% [19–21]. However, such a “two-step” method complicates the technological process when considering a potential industrial application. In this regard, a single bifunctional catalyst with both acid and redox sites is preferable to allow a “one-pot” and “one-step” route.



Scheme 1. Reaction scheme for the “one-pot” fructose-to-2,5-diformylfuran (DFF) transformation.

The reported bifunctional catalysts included the cesium salts of Mo- or Mo–V-containing Keggin heteropolyacids [22,23], graphene oxide [24], sulfonated amine-functionalized carbonaceous catalyst (CC-SO₃H-NH₂) [25], Mo- or V-containing composite catalysts (e.g., f-Ce₉Mo₁O₈ [26], Mo-HNC [27], sulfonated MoO₃-ZrO₂ [28], V₂O₅@MOR [29], and V-g-C₃N₄(H⁺) [30]), and magnetic acid catalysts (e.g., Fe₃O₄@C-SO₃H [31] and WO₃HO-VO(salten)-SiO₂@Fe₃O₄ [32]). Relatively higher DFF yields (70~86%) have been obtained by conducting the fructose dehydration under a nitrogen atmosphere while subsequent oxidation under oxygen atmosphere [24–26,32–35], wherein the fructose oxidation could be reduced while a long reaction time of 11~24 h was required. In addition to the larger energy input, such a long reaction time also resulted in further oxidation of DFF to 5-formyl-2-furancarboxylic (FFCA) and/or 2,5-furandicarboxylic acid (FDCA) (Scheme 1), which undoubtedly increases the separation energy of the target product DFF. To lower the energy consumption for this “one-pot” and “one-step” fructose-to-DFF transformation, effective bifunctional solid catalysts are still needed.

An effective bifunctional catalyst is deemed to allow fast fructose dehydration and rapid HMF oxidation so as to minimize the possible parallel or tandem side-reactions from fructose and HMF, even in the presence of water. Among others, the Mo-containing catalysts have exhibited higher selectivity for fructose dehydration without nitrogen protection during the fructose-to-DFF conversion owing to the moderate redox performance of Mo-containing species [22,27,36]. The anchoring of Mo-containing active species onto a suitable organic “support” might retain their high selectivity while endowing an extra catalytic performance derived from the organic “support”. Notably, polyaniline (PAN) has recently received particular interest in catalytic applications as a heterogeneous organic support owing to its facile synthesis, air-stable performance, good dispersion of active species, and the pseudo-homogeneous character in organic solvents [20,37–44]. In our group, we found that the functionalized PANs exhibited promising catalytic performance towards the dehydration of fructose into furans [45–47]. Considering the advantages and characteristics of PAN, we are expecting to incorporate the Mo-involved redox sites into the PAN “supports” such that the bifunctions of oxidation and dehydration could be combined, and even strengthened in a single inorganic-organic hybrid catalyst. Despite the heterogeneity of the hybrid catalyst, the catalytic performance for the tandem

fructose-to-HMF dehydration and HMF-to-DFF oxidation are expected to be promoted in one-pot whereas the side reactions might be alleviated as much as possible.

In this work, we report the preparation of bifunctional inorganic–organic hybrid catalysts by supporting keggin-type $\text{H}_3\text{PMo}_{12}\text{O}_{40}$ (PMo_{12}) heteropolyacid (HPA) on PAN or formyl-functionalized PAN (F-PAN) for the “one-pot” and “one-step” synthesis of DFF from fructose. The morphology, composition, structure, and thermostability of the as-prepared $\text{PMo}_{12}/\text{PAN}$ and $\text{PMo}_{12}/\text{F-PAN}$ catalysts are characterized by transmission electron microscope (TEM), scanning electron microscope (SEM)/energy dispersive X-ray spectroscopy (EDX) mapping, inductively coupled plasma-atomic emission spectroscopy (ICP-AES), Fourier transform infrared spectroscopy (FTIR), x-ray diffraction (XRD), and thermogravimetric (TG) analysis. The catalytic performances and reusability of these hybrid catalysts are studied for both HMF-to-DFF oxidation and the “one-pot” “one-step” fructose-to-DFF transformation.

2. Results and Discussion

2.1. Preparation and Characterization of $x\text{-PMo}_{12}/\text{PAN}$ Catalysts

The Keggin-type PMo_{12} HPA was synthesized according to the literature [48], and the formation of the Keggin structure was confirmed by FTIR and XRD spectra (Figure S1). The sulfates of PAN were synthesized by oxidative polymerization of aniline with ammonium persulfate in dilute aqueous sulfuric acid at 278 K [45,49]. The “support” PAN was then synthesized by deprotonating the PAN sulfates with aqueous ammonia at room temperature. The FTIR spectrum of PAN (Figure 1a, i) illustrated the formation of para-polymerized PAN owing to the appearance of the characteristic band centered at 826 cm^{-1} assigned to the C–H out-of-plane bending in the 1,4-disubstituted ring structure of PAN [50]. The IR bands centered at 1495 and 1588 cm^{-1} respectively corresponded to the C=C ring stretching vibration of benzenoid and quinone rings in PAN [51,52]. Besides, the IR band at 1160 cm^{-1} was assigned to the C–C aromatic in-plane bending of PAN [53], and the band at 1295 cm^{-1} originated from the C–N stretching vibration of the secondary aromatic amine [54,55]. The XRD pattern of PAN (Figure 1b, i) showed a typical amorphous structure of deprotonated PAN with a broad diffraction peak ranging from 2θ of $15\sim 25^\circ$ [56,57].

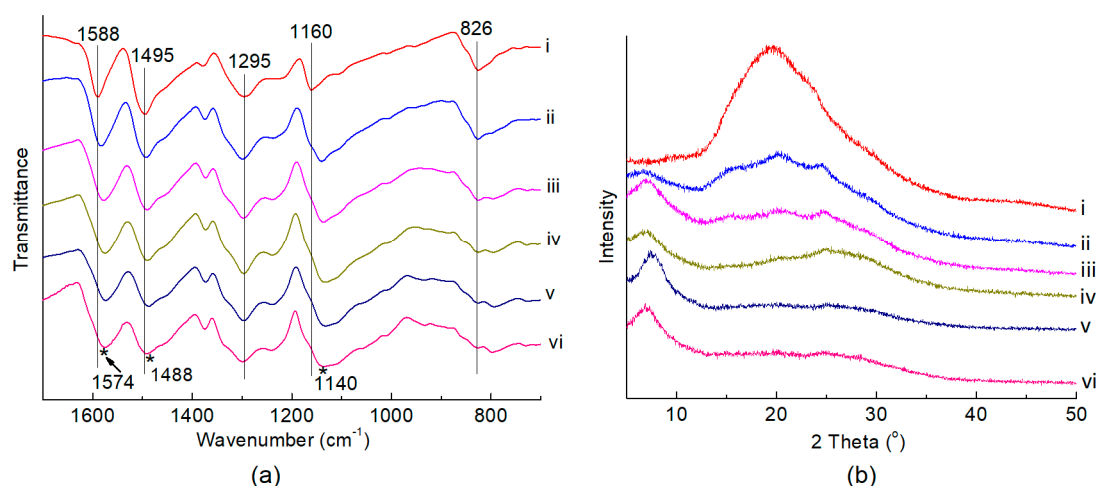
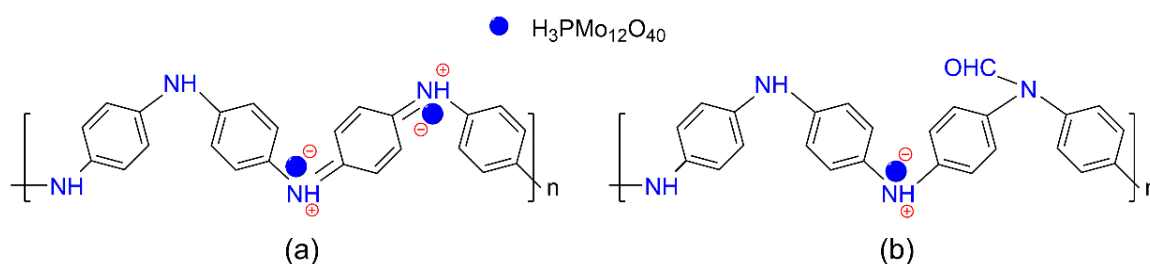


Figure 1. (a) FTIR spectra and (b) XRD patterns of the polyaniline (PAN) and $x\text{-PMo}_{12}/\text{PAN}$ catalysts. (i) PAN; (ii) $10\text{-PMo}_{12}/\text{PAN}$; (iii) $20\text{-PMo}_{12}/\text{PAN}$; (iv) $30\text{-PMo}_{12}/\text{PAN}$; (v) $40\text{-PMo}_{12}/\text{PAN}$; (vi) $50\text{-PMo}_{12}/\text{PAN}$.

A series of $x\text{-PMo}_{12}/\text{PAN}$ ($x = 10\sim 50$) catalysts were prepared by impregnating PAN in an aqueous ethanol solution ($V_{\text{C}_2\text{H}_5\text{OH}}/V_{\text{H}_2\text{O}} = 1/1$) containing PMo_{12} HPA, wherein x represented the theoretical weight loading of HPA. The FTIR spectra of the $x\text{-PMo}_{12}/\text{PAN}$ catalysts (Figure 1a, ii–vi) exhibited

obvious shifts from 1495 to 1488 cm^{-1} and 1588 to 1574 cm^{-1} , which were indicative of the protonation of PAN with HPA [58]. As proof, a broad and overlapping IR band at around 1100–1200 cm^{-1} appeared, which corresponded to the $-\text{N}=\text{quinoid}=\text{N}-$ (electronlike band) stretching modes and often related to the protonated structure of PAN [59]. That is, the “support” PAN has been protonated with PMo_{12} HPA, most possibly via the acid–base interaction between the quinoid diimine structure in PAN and the protons in PMo_{12} HPA (Scheme 2a). However, the characteristic IR bands of PMo_{12} HPA centered at 1064, 965, 870, and 787 cm^{-1} were obscure owing to their overlaps by the strong IR bands of PAN [60]. The XRD patterns of the $x\text{-PMo}_{12}$ /PAN catalysts (Figure 1b, ii~vi) showed a new and broad diffraction peak at $2\theta = 5\sim 10^\circ$ assigned to the protonated PAN structure with increasing HPA loadings [56], thereby further confirming the anchoring of HPA on PAN. Nevertheless, these hybrid catalysts are still in amorphous structures. The ICP-AES analysis of the $x\text{-PMo}_{12}$ /PAN catalysts revealed that the actual HPA loading on the hybrid catalysts ranged from 8.4 to 38.5 wt.% (Table 1, entry 1~5). The absence of typical diffraction peaks of PMo_{12} HPA on the XRD patterns of the as-prepared $x\text{-PMo}_{12}$ /PAN catalysts was indicative of the good dispersion of HPA on the $x\text{-PMo}_{12}$ /PAN catalysts, which might benefit from the site-to-site acid–base interaction during HPA anchoring. As proof, we observed the morphologies of PAN and 40- PMo_{12} /PAN catalyst by TEM (Figure S2), and found that they both existed in a sheet shape. Although no characteristic aggregation of HPA crystal was observed on the TEM and SEM images of the 40- PMo_{12} /PAN catalyst, the EDX-mapping of this catalyst strongly revealed the well-dispersion of HPA on the organic PAN support (Figure 2).



Scheme 2. Possible structures of (a) PMo_{12} /PAN, and (b) PMo_{12} /F-PAN catalysts. The PMo_{12} heteropolyacid (HPA) interacts with the organic supports by site-to-site acid–base interaction between the quinoid diimine structure in PAN (or F-PAN) and the protons in PMo_{12} HPA.

Table 1. Catalytic performance of several PMo_{12} -containing catalysts in the aerobic oxidation of 5-hydroxymethylfurfural (HMF) to DFF ^a.

Entry	Cat.	Actual Loading of HPA (wt.%) ^b	Conv. (mol%) ^c	Y_{DFF} (mol%) ^c	Carbon Balance (mol%) ^c
1	10- PMo_{12} /PAN	8.4	56.5 (13.1)	53.6 (12.3)	97.1 (99.2)
2	20- PMo_{12} /PAN	15.6	75.6 (15.0)	74.9 (14.7)	99.3 (99.7)
3	30- PMo_{12} /PAN	26.2	96.5 (16.1)	91.5 (15.2)	95.0 (99.1)
4	40- PMo_{12} /PAN	31.3	97.2 ^d (33.2)	94.0 ^e (31.6)	96.8 (98.4)
5	50- PMo_{12} /PAN	38.5	100.0 (26.6)	91.2 (24.7)	91.2 (98.1)
6 ^f	PMo_{12} HPA	-	100.0	96.0	96.0
7 ^g	PAN	-	21.0	14.4	93.4
8 ^h	40- PMo_{12} /F ₃ -PAN	30.6	60.0	58.4 ⁱ	98.4

^a Reaction conditions: 35 mg HMF, 30 mg catalyst, 1 mL DMSO, 433 K, 4 h, in air. ^b Actual PMo_{12} loadings obtained by ICP-AES analysis. ^c The values in parentheses represent the data obtained after 1 h's reaction. ^d The conversions of HMF were all 100% for the second, third, and fourth catalytic runs. ^e The yields of DFF were 94.7%, 93.5%, and 94.1%, respectively, for the second, third, and fourth catalytic runs. ^f 9 mg PMo_{12} HPA was used. ^g 21 mg PAN was used. ^h 5 mg 40- PMo_{12} /F₃-PAN was used as a catalyst in the presence of water (13.5 mg). ⁱ FA (1.5 mol%) was generated as a by-product.

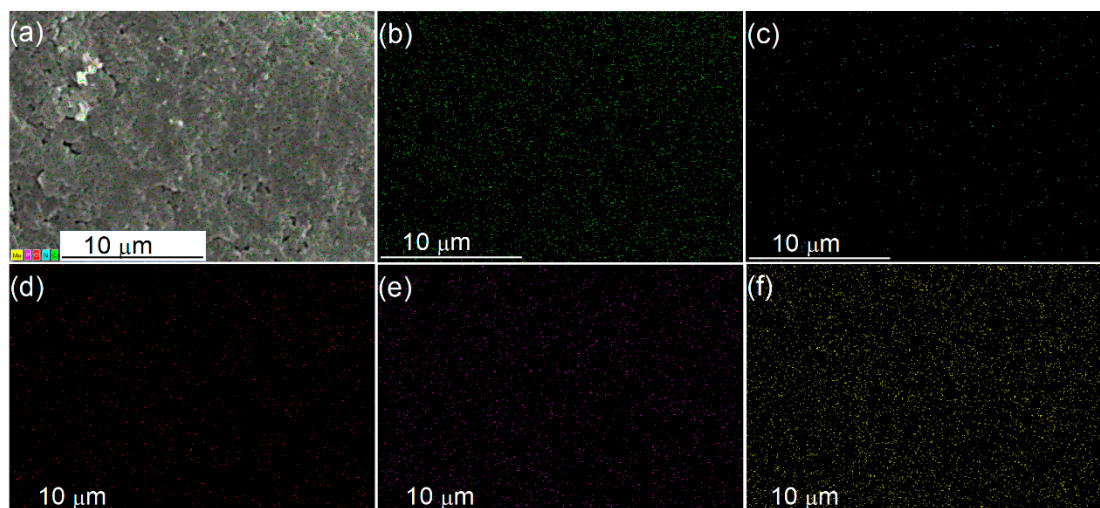


Figure 2. SEM/EDX-mapping of the 40-PMo₁₂/PAN catalyst. (a) SEM photo, (b) C element, (c) N element, (d) O element, (e) P element, and (f) Mo element.

2.2. Aerobic Oxidation of HMF to DFF over *x*-PMo₁₂/PAN Catalysts

The catalytic performance of the *x*-PMo₁₂/PAN catalysts in the aerobic oxidation of HMF to DFF at 433 K for 1 h and 4 h is depicted in Table 1. After 1 h's reaction, both the HMF conversion and the DFF yield increased with an increase of the PMo₁₂ loadings from 8.4 wt.% (10-PMo₁₂/PAN) to 31.3 wt.% (40-PMo₁₂/PAN) (entry 1~4), reaching the maximum values at 33.2 mol% and 31.6 mol%, respectively. However, a further increase of the HPA loading to 38.5 wt.% over 50-PMo₁₂/PAN catalyst resulted in the decrease of both HMF conversion (26.6 mol%) and DFF yield (24.7 mol%) (entry 5), possibly owing to the aggravation of humins generation as a result of the increase of Brønsted acidity on the hybrid catalyst. The prolonging of the reaction time to 4 h gave similar product distributions, wherein a maximum DFF yield of 94.0 mol% was obtained over the 40-PMo₁₂/PAN catalyst (entry 4). It was noted that neither FA and LA nor FFCA and FDCA were detected over all these hybrid catalysts. In all cases, the carbon balances were higher than 91.2%, thereby representing a good catalytic performance of the *x*-PMo₁₂/PAN catalysts for the aerobic oxidation of HMF to DFF. In contrast experiments, the aerobic oxidation of HMF over PMo₁₂ HPA at 433 K for 4 h produced a similar high DFF yield of 96.0 mol% with complete conversion of HMF (entry 6), while the oxidation over PAN just led to a DFF yield of 14.4 mol% with HMF conversion of 21.0 mol% (entry 7). It was obvious that the loading of the PMo₁₂ HPA on PAN improved the catalytic performance of the hybrid catalysts for the HMF-to-DFF oxidation. However, the comparison of the performance enhancement revealed that the PMo₁₂ HPA was the main active species for HMF oxidation. Notably, the heterogeneous 40-PMo₁₂/PAN catalyst showed good reusability for aerobic oxidation of HMF to DFF in successive four catalytic runs with DFF yield and selectivity less than 93.5% (entry 4).

2.3. One-pot and One-step Conversion of Fructose to DFF over 40-PMo₁₂/PAN Catalyst

The PMo₁₂ HPA was itself a homogeneous inorganic catalyst for the tandem fructose-to-HMF dehydration and HMF-to-DFF oxidation due to the co-existence of Brønsted acid sites and redox Mo⁶⁺ species in structure [22]. However, the direct use of PMo₁₂ HPA in this one-pot reaction (433 K, 4 h) led to the generation of a large amount of FA (28.0 mol%) and small amount of furfural (FF, 3.5 mol%) in addition to DFF (61.0 mol%) (Table 2, entry 1). The anchoring of the PMo₁₂ HPA onto the PAN "support" resulted in the decreases of DFF yield to 49.6 mol%, FF yield to 1.6 mol%, and FA yield to 19.5 mol% over 40-PMo₁₂/PAN (entry 2). Meanwhile, the carbon balance for this fructose-to-DFF transformation was decreased to 60.0~69.5 mol% (entry 1~5). The loss of the product yields and the carbon balance might originate from the reduction of the Brønsted acidity of the hybrid catalyst owing to the acid–base interaction between the protons in HPA and the quinoid diimine structure in

PAN. Although the catalytic performance of the fresh 40-PMo₁₂/PAN catalyst was relatively lower, the reuse of this catalyst in successive runs produced notably higher DFF yields ranging from 58 to 68 mol% accompanying with the decrease of FA yield to about 9 mol% (entry 3–5). To reveal the possible deactivation or activity strengthening of the 40-PMo₁₂/PAN catalyst during the recycling process, in contrast, experiments, the one-pot conversions of fructose were performed at 433 K for only 1 h. The results shown in Table 2 also indicated the obvious increase of both HMF and DFF yields for the second, third, and fourth catalytic runs when compared with the first catalytic run, thereby strongly demonstrating the strengthening of the dehydration performance for the used 40-PMo₁₂/PAN catalysts. The FTIR spectrum (Figure S3a) of the used catalyst exhibited a new IR band centered at 1669 cm⁻¹ originating from the stretching vibration of the aldehyde group, which was indicative of the possible absorption of intermediate HMF and product DFF, or the grafting of formyl groups on the diimine nitrogen of PAN during the fructose conversion [45]. The possibility of HMF and DFF absorption on the used catalyst was excluded because the FTIR spectra of the 40-PMo₁₂/PAN catalysts after interacting with HMF or DFF produced a different IR band at 1662 and 1664 cm⁻¹ (Figure S3c,d), respectively. Furthermore, the FTIR spectrum of the 40-PMo₁₂/PAN catalyst after its interaction with formaldehyde under similar experimental conditions in the absence of fructose was similar to that of the used 40-PMo₁₂/PAN catalyst (Figure S3b), thereby demonstrating the occurrence of formyl grafting on the 40-PMo₁₂/PAN catalyst during the fructose-to-DFF transformation. As shown in Scheme S1, the formal grafting might occur on the quinone diimine site, resulting in the formation of an amide structure in the polymer chain [45]. Here, the formaldehyde was generated from the direct decomposition of fructose accompanied by the formation of FF [61,62].

Table 2. Catalytic performance of several catalysts in the “one-pot” and “one-step” conversion of fructose to DFF. ^a

Entry	Cat.	Actual Loading of HPA (wt.%) ^b	Conv. (mol%) ^c	Y _{HMF} (mol%) ^c	Y _{DFF} (mol%) ^c	Y _{FA} (mol%) ^c	Carbon Balance (mol%) ^c
1 ^d	PMo ₁₂ HPA	-	100	-	61.0	28.0	65.7
2	40-PMo ₁₂ /PAN	31.3	100 (96.5)	2.9 (21.2)	49.6 (23.9)	19.5 (8.4)	55.8 (48.1)
3 ^e	40-PMo ₁₂ /PAN	31.3	100 (96.6)	- (30.5)	58.0 (30.5)	12.0 (4.2)	60.0 (63.9)
4 ^f	40-PMo ₁₂ /PAN	31.3	100 (97.6)	- (30.7)	68.0 (31.4)	9.0 (4.5)	69.5 (63.6)
5 ^g	40-PMo ₁₂ /PAN	31.3	100 (96.5)	- (37.9)	65.0 (31.2)	9.0 (3.8)	66.5 (72.3)
6 ^h	40-PMo ₁₂ /F ₁ -PAN	19.6	100	36.5	42.3	3.1	79.3
7 ^h	40-PMo ₁₂ /F ₂ -PAN	22.9	100	12.0	64.5	6.6	77.6
8 ^h	40-PMo ₁₂ /F ₃ -PAN	30.6	100	9.7	67.1	5.5	77.7

^a Reaction conditions: 45 mg fructose, 30 mg catalyst, 1 mL DMSO, 433 K, 4 h, in air. ^b Actual PMo₁₂ loadings obtained by ICP-AES analysis. ^c The values in parentheses represent the data obtained after 1 h's reaction. ^d 9 mg PMo₁₂ HPA was used. ^e The second catalytic run. ^f The third catalytic run. ^g The fourth catalytic run. ^h 5 mg 40-PMo₁₂/F_y-PAN catalysts were used.

2.4. Preparation and Characterization of 40-PMo₁₂/F_y-PAN Catalysts

In order to enhance the stability of the hybrid catalyst during the fructose conversion, the “support” PAN was modified by treating with various amount of formaldehyde at 413 K for 2 h before anchoring with PMo₁₂ HPA. The as-prepared solid powders were named F_y-PAN and characterized by FTIR spectra (Figure 3a, i~iii), wherein the appearance of IR band centered at 1675 cm⁻¹ suggested the successful grafting of formyl groups on PAN [45]. Moreover, the relative peak intensity of 1675 cm⁻¹ to 820 cm⁻¹ (I_{1675}/I_{820}) on the FTIR spectra could be used to represent the grafting level of the formyl groups on F_y-PAN, and I_{1606}/I_{1502} could be used to evaluate the relative content of the quinoid diimine and benzene ring structure [54]. As shown in Table S1, the grafting of formyl groups on F_y-PAN resulted in the decrease of I_{1606}/I_{1502} (entry 1~3) when compared with that on PAN (entry 4), which was consistent with our previous work that demonstrated that the formaldehyde modification of PAN led to the reduction of quinoid diimine structure to phenylenediamine structure on the polymer chain [45].

Besides, we found that the grafting level of the formyl groups on F_y-PAN decreased with increasing the amount of formaldehyde used for modification.

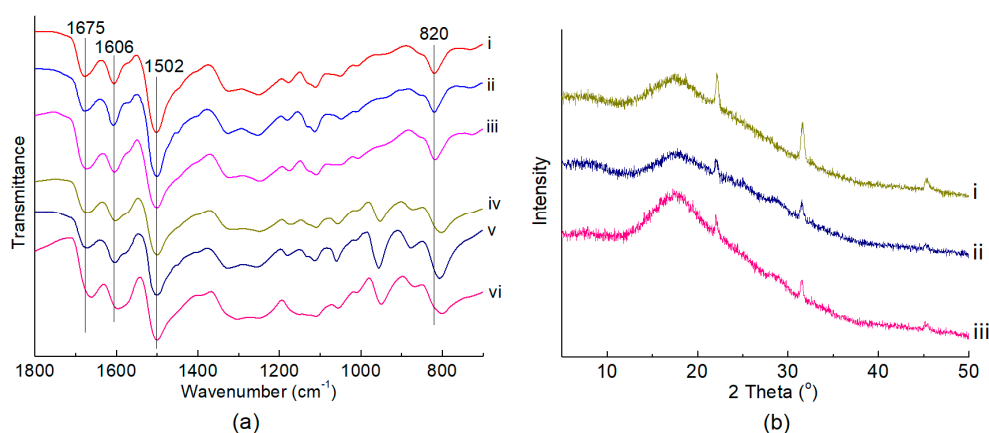


Figure 3. (a) FTIR spectra of F_y-PAN and 40-PMo₁₂/F_y-PAN. (i) F₁-PAN, (ii) F₂-PAN, (iii) F₃-PAN, (iv) 40-PMo₁₂/F₁-PAN, (v) 40-PMo₁₂/F₂-PAN, (vi) 40-PMo₁₂/F₃-PAN. (b) XRD patterns of 40-PMo₁₂/F_y-PAN catalysts. (i) 40-PMo₁₂/F₁-PAN; (ii) 40-PMo₁₂/F₂-PAN; (iii) 40-PMo₁₂/F₃-PAN.

After anchoring with PMo₁₂ HPA (40 wt.%), the actual HPA loadings on these PMo₁₂/F_y-PAN catalysts varied, increasing from 19.6 wt.% on PMo₁₂/F₁-PAN, 22.9 wt.% on PMo₁₂/F₂-PAN, to 30.6 wt.% on PMo₁₂/F₃-PAN (Table 2), although the theoretical HPA loading was kept unchanged at 40 wt%. These results indicated that the lower grafting level of formyl groups on F_y-PAN “support” was beneficial for loading the PMo₁₂ HPA because both the formyl grafting and HPA anchoring occurred on the quinoid diimine sites. The possible chemical structure of the PMo₁₂/F_y-PAN catalysts is shown in Scheme 2b. The FTIR spectra (Figure 3a, iv~vi) demonstrated that the formyl groups on F_y-PAN were stable during the HPA anchoring. The XRD patterns of the as-prepared PMo₁₂/F_y-PAN catalysts (Figure 3b) revealed the partial crystallization of these hybrid catalysts owing to the appearance of sharp diffraction peaks at 2θ of 22° and 32° [56]. The reason for the formation of the partially crystallized species is unclear, requiring deep characterization in our future work. Nevertheless, the PMo₁₂ species were still well-dispersed on the F_y-PAN “support” because no typical diffraction peaks assigning to crystallized PMo₁₂ HPA were observed on the XRD patterns and no obvious HPA crystals were observed on their TEM images (Figure S4). Meanwhile, this well-distribution of the PMo₁₂ species was further supported by the EDX-mapping of the PMo₁₂/F_y-PAN catalyst (Figure 4).

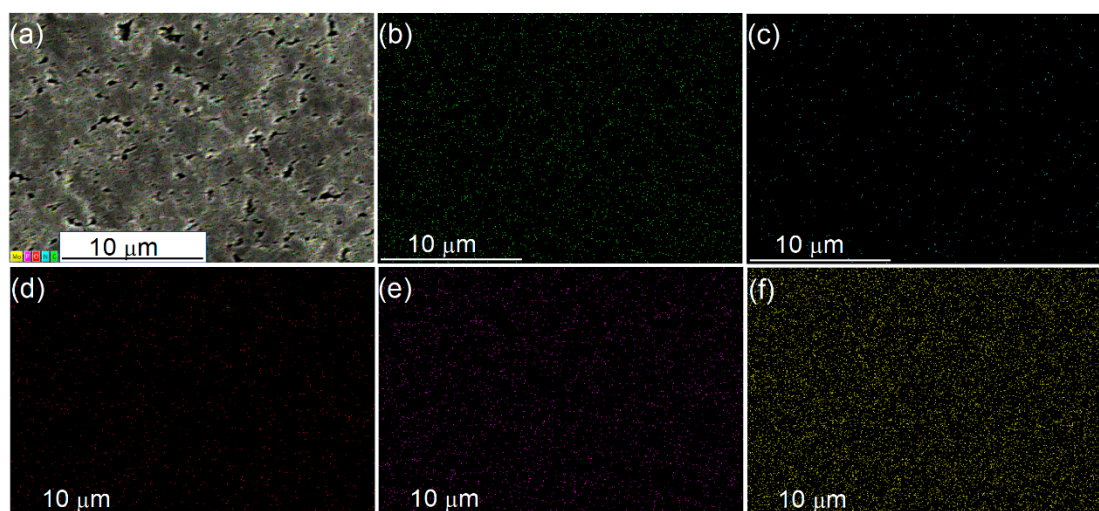


Figure 4. SEM/EDX-mapping of the 40-PMo₁₂/F₃-PAN catalyst. (a) SEM photo, (b) C element, (c) N element, (d) O element, (e) P element, and (f) Mo element.

2.5. One-pot and One-step Conversion of Fructose to DFF over 40-PMO₁₂/F_y-PAN Catalysts

The catalytic performance of the 40-PMO₁₂/F_y-PAN catalysts in the direct conversion of fructose to DFF is depicted in Table 2 (entry 6–8). With increasing the HPA loadings, the DFF yields increased from 42.3 mol% over 40-PMO₁₂/F₁-PAN to 67.1 mol% over 40-PMO₁₂/F₃-PAN. It was noted that the total yields of HMF and DFF, representing the total dehydration performance of the catalysts, were comparable for all 40-PMO₁₂/F_y-PAN catalysts, whereas higher than that of the 40-PMO₁₂/PAN catalyst (~77.4 mol% v.s. 52.5 mol%). The carbon balance was increased to approach 80.0 mol% over these 40-PMO₁₂/F_y-PAN catalysts. That is, the grafting of formyl groups on PAN before anchoring the PMO₁₂ HPA promoted the catalytic dehydration performance of the 40-PMO₁₂/F_y-PAN hybrid catalysts, thereby illustrating that the F_y-PAN acts as a “support” for anchoring and dispersing PMO₁₂ species as well as a co-catalyst for reinforcing the dehydration performance of the PMO₁₂/F_y-PAN hybrid catalysts. Moreover, the production rates, expressed as (mol of DFF)/(mol of PMO₁₂ HPA), are comparatively shown in Table S2. The results revealed that the production rate of DFF on 40-PMO₁₂/F_y-PAN catalysts was higher than the 40-PMO₁₂/PAN catalyst, which strongly confirmed the reinforcement of the catalytic performance by the F_y-PAN support. In all cases, no LA was detected while FA formed with lower yields ranging from 3.1 to 6.6 mol%, which suggested that the FA came from direct degradation of fructose or HMF instead of from HMF rehydration. That is, the HMF rehydration during the “one-pot” and “one-step” fructose-to-DFF transformation over the 40-PMO₁₂/F_y-PAN hybrid catalysts has been completely inhibited whereas the fructose or HMF degradation to FA has been significantly reduced, thus avoiding the unfavorable impact of water on the tandem fructose-to-DFF reactions.

In addition, we found that the highest DFF yield of 99.9 mol% could be achieved when conducting the aerobic oxidation of HMF over the 40-PMO₁₂/F₃-PAN catalyst for 5 h (Figure 5a). In another contrast experiment, the oxidation of HMF over the 40-PMO₁₂/F₃-PAN catalyst in the presence of water resulted in a high DFF selectivity of 97.3%, where a small amount of FA (1.5 mol%) formed as the by-product from HMF degradation (Table 1, entry 8). These results demonstrated that the 40-PMO₁₂/F₃-PAN catalyst was highly selective towards the HMF-to-DFF oxidation, even in the presence of water.

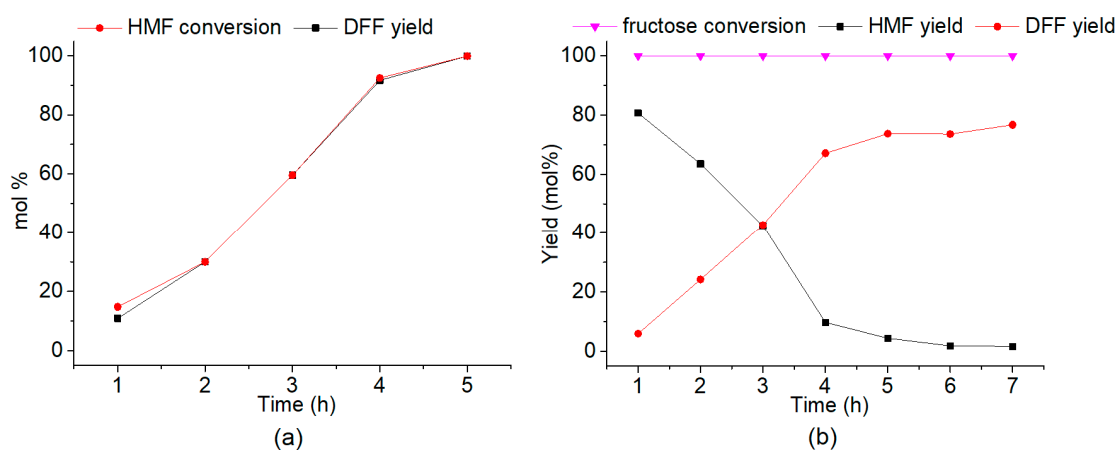


Figure 5. (a) Time profile for the aerobic oxidation of HMF to DFF over the 40-PMO₁₂/F₃-PAN catalyst. (b) Time profile for the “one-pot” and “one-step” conversion of fructose to DFF over the 40-PMO₁₂/F₃-PAN catalyst. Reaction conditions: 35 mg HMF or 45 mg fructose, 5 mg 40-PMO₁₂/F₃-PAN catalyst, 1 mL DMSO, 433 K, in air.

Notably, over the bifunctional 40-PMO₁₂/F₃-PAN catalyst, the DFF yields in the “one-pot” and “one-step” fructose-to-DFF transformation could be increased to 76.7 mol% by prolonging the reaction time to 7 h (Figure 5b). This bifunctional hybrid catalyst produced higher or considerable DFF yields to the Cs₃HfPMo₁₁VO₄₀ [23], graphene oxide [24], f-Ce₉Mo₁O₈ [26], sulfonated MoO₃-ZrO₂ [28], and Ru/H-beta [33] catalysts, especially by shortening the reaction time to 7 h (Table 3). Although the catalytic performance of our hybrid catalyst was relatively lower than those of the

V₂O₅@MOR(+HCl) [29], Au-Ru/rGO [34], and Co/Al hydrotalcites [35] catalysts, the use of liquid acid catalyst and/or the switching of the reaction atmosphere have been avoided in our work. Significantly, this inorganic–organic hybrid catalyst showed higher activity for DFF formation when compared with our previously reported Cs_{0.5}H_{2.5}PMo₁₂O₄₀ catalyst because of the strengthening of the dehydration performance by the organic “support”. Furthermore, the site time yield (STY) of DFF, expressed as (mol of DFF)/(g of catalyst)/h, are also compared in Table 3. The bifunctional hybrid catalyst exhibits higher STY than most of the reported catalysts except the Cs_{0.5}H_{2.5}PMo₁₂O₄₀ [22] and sulfonated MoO₃-ZrO₂ [28] catalysts, possibly due to the smaller amount of active sites in the hybrid catalyst.

Table 3. Catalytic performance comparison of the bifunctional hybrid catalyst with those reported in the literature for the “one-pot” fructose-to-DFF transformation.

Entry	Catalyst	T (K)	Time (h)	Conv. (mol%)	Y _{HMF} (mol%)	Y _{DFF} (mol%)	STY of DFF (× 10 ⁻³ mol/g/h) ^c	Ref.
1	Cs _{0.5} H _{2.5} PMo ₁₂ O ₄₀	433	4	100	0.2	69	8.6	[22]
2	Cs ₃ HPMo ₁₁ VO ₄₀	393	2 + 6 ^a	99	2	60	0.6	[23]
3	Graphene oxide	413	2 + 22 ^a	- ^b	- ^b	72	3.0	[24]
4	f-Ce ₉ Mo ₁ O ₈	393	2 + 10 ^a	100	- ^b	74	0.7	[26]
5	Sulfonated MoO ₃ -ZrO ₂	423	10	100	- ^b	74	8.2	[28]
6	V ₂ O ₅ @MOR (+HCl)	393	4 + 12 ^a	100	0.1	96	0.2	[29]
7	Ru/H-beta	393	24	100	- ^b	80	0.3	[33]
8	Au-Ru/rGO	383	2 + 6 ^a	100	- ^b	86	2.7	[34]
9	Co/Al hydrotalcites	393	2 + 6 ^a	100	- ^b	87	2.2	[35]
10	PMo ₁₂ /F-PAN	433	7	100	1.6	76.7	5.5	This work

^a The respective reaction time applied for the fructose-to-HMF dehydration under nitrogen atmosphere and the subsequent HMF-to-DFF oxidation under oxygen atmosphere. ^b Not mentioned in literatures. ^c The site time yield of DFF (mol of DFF/g of catalyst/h).

Although about 1.5~3.0% of the PMo₁₂ species leached from the 40-PMo₁₂/F₃-PAN catalyst (Table S3), we found that the 40-PMo₁₂/F₃-PAN hybrid catalyst could be reused for at least four catalytic runs with DFF yield no less than 63.0 mol% for 4 h's reaction (Figure 6a). In comparison, the recycling experiments were carried out for only 0.2 h or 1.0 h to investigate the possible deactivation of the 40-PMo₁₂/F₃-PAN catalyst (Table S4). For the reaction of 0.2 h, the fructose conversions were similar (41.9~43.5 mol%) for the successive four catalytic runs with similar HMF yields ranging from 36.9 mol% to 37.9 mol% and a trace amount of DFF formed, which suggested a stable catalytic performance of the 40-PMo₁₂/F₃-PAN catalyst for the fructose-to-HMF dehydration. In the meantime, the fructose conversion was performed with a smaller stirring speed of 50 rpm. A similar HMF yield of 37.7 mol% was obtained as compared with that under a faster stirring speed of 400 rpm, thereby revealing the insignificance of the mass transfer limitation in the catalytic tests. Increasing the reaction time to 1.0 h resulted in the increase of the fructose conversion to nearly 100 mol% with HMF formed as the major product and DFF as the minor product. This result indicated that the rate of fructose-to-HMF dehydration was very fast, whereas the oxidation was relatively slower. Nevertheless, the considerable total yields of HMF and DFF (70.0~75.6 mol%) in the recycling tests for 1 h demonstrated the good reusability of the 40-PMo₁₂/F₃-PAN catalyst during the recycling tests. Moreover, the heterogeneity of the hybrid catalyst could be ensured because the leached PMo₁₂ species contributed little to the fructose-to-DFF conversion. Lower DFF yields of 4.9~5.0 mol% were obtained by using the leached PMo₁₂ species as the catalyst (Table S3). The FTIR spectra of the spent 40-PMo₁₂/F₃-PAN catalysts after the first and fourth catalytic runs (Figure 6b) were similar to that of the fresh one, which illustrated the stability of the inorganic-organic hybrid catalyst under the experimental conditions. A further TG study of the fresh and spent 40-PMo₁₂/F₃-PAN catalysts showed that both catalysts began to decompose at 598~620 K (Figure S5), which demonstrated the thermostability of the 40-PMo₁₂/F₃-PAN catalyst under the experimental conditions.

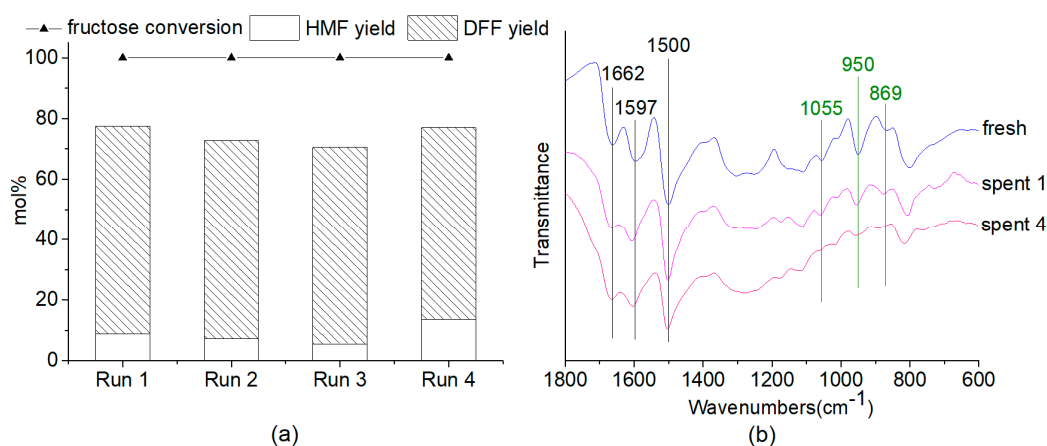


Figure 6. (a) Recycled use of 40-PMo₁₂/F₃-PAN catalyst in the “one-pot” and “one-step” fructose-to-DFF conversion. (b) FTIR spectra of the fresh and spent 40-PMo₁₂/F₃-PAN catalysts. Spent 1 represents the used catalyst after the first catalytic run; Spent 4 represents the used catalyst after the fourth catalytic run. Reaction conditions: 45 mg fructose, 30 mg catalyst, 1 mL DMSO, 433 K, 4 h, in air.

3. Materials and Methods

3.1. Materials

HMF (98%), DFF (98%), LA (98%), and FA (98%) were purchased from J&K chemical co., Ltd. (Beijing, China). Fructose (98%), FFCA (>98%), and FDCA (97%) were purchased from Tokyo Chemical Industry (Tokyo, Japan). DMSO (99%), sulfuric acid (98%), formaldehyde (40 wt.%), aqueous ammonia (25~28 wt.%), and analytical reagent (AR) grade of ethyl ether, aniline, and ammonium persulfate were purchased from Kolong chemical company (Chengdu, China). Na₂HPO₄ and Na₂MoO₄ in AR grade were purchased from Chengdu Chemical Reagent Company (Chengdu, China) and Tianjin Chemical Reagent Company (Tianjin, China), respectively. Aniline was distilled before use. All of the other chemical reagents were used as purchased without further purification. Ultrapure water (resistance = 18.25 MΩ cm⁻¹) was used in all of our experiments.

3.2. Methods

3.2.1. Catalyst Preparation

The Keggin-type PMo₁₂ HPA was synthesized as follows: Na₂HPO₄ (74.0 g/L, 100 mL) and Na₂MoO₄ (295.0 g/L, 200 mL) were mixed and heated to boiling for 30 min. After being cooled down to room temperature, the mixture was dropped slowly with concentrated H₂SO₄ with vigorous stirring until the pH of the mixture reached 2, giving out a yellow mixture containing PMo₁₂ HPA. The PMo₁₂ HPA was then extracted with ethyl ether (300 mL). After separation, a stream of air was passed through the heteropoly etherate layer (upper layer) to get the crude orange solid. This solid was then dissolved in a small amount of water, concentrated to the appearance of crystals in a vacuum desiccator, and allowed to be crystallized further. The resultant yellow solid powder was dried at 353 K for 10 h.

PAN was prepared as follows: Freshly distilled aniline (8.2 mg) was dissolved in aqueous H₂SO₄ solution (0.8 M, 400 mL) at 278 K and kept stirring for 30 min. A solution of ammonium persulfate (170.0 g/L, 160 mL) was dropped into the above mixture solution at 278 K within 20 min, and then kept stirring at this temperature for another 40 min. The resulting precipitate (i.e., the sulfate of PAN) was separated by filtration, washed with water (100 mL × 4), and then dried at 353 K for 10 h. The PAN sulfate (2.0 g) was then dissolved in aqueous ammonia (40 mL) and the mixture was stirred at room temperature for 2 h. After the reaction, the solid was filtrated, washed with water (100 mL × 4), and then dried at 353 K for 10 h. To obtain the F_y-PAN support, the PAN sulfate (0.2 g) was dissolved

in aqueous formaldehyde solution (15~40 wt.%, 8~15 mL), followed by being heated to 413 K and kept stirring for 2 h. After the completion of the reaction, the solid was filtrated, washed with water (20 mL \times 3), and then dried at 353 K for 10 h.

x -PMo₁₂/PAN and x -PMo₁₂/F_Y-PAN catalyst were prepared by impregnating PAN or F_Y-PAN in aqueous ethanol solution ($V_{C_2H_5OH}/V_{H_2O} = 1/1$) containing PMo₁₂ HPA, wherein x (10~50) represented the theoretical mass ratio between HPA and (PAN+HPA) used. In a typical synthesis of 40-PMo₁₂/PAN catalyst, PAN (0.24 g) was dissolved in the PMo₁₂ HPA solution (4.0 g/L, 40 mL) and the mixture was stirred at room temperature for 12 h. After the reaction, the as-prepared solid was filtrated, washed water (10 mL \times 3), and was dried at 353 K for 10 h.

3.2.2. Catalyst Characterization

The FTIR spectra were recorded by a Nicolet Nexus 6700 spectrometer (Boston, MA, USA) with a spectral resolution of 4 cm⁻¹ in the wavenumber range of 500~4000 cm⁻¹ at room temperature. The XRD patterns were collected by a PANalytical Empyrean powder X-ray diffraction instrument (Almelo, Netherlands) operating at 40 kV and 25 mA with nickel-filtered CuK α radiation ($\lambda = 1.54056 \text{ \AA}$), wherein the data of $2\theta = 5\text{--}50^\circ$ with a step of 0.0544 $^\circ$ were recorded. The ICP-AES were conducted on a VG PQExCell instrument (TJA, Boston, MA, USA). The TEM images were obtained on an FEI Tecnai G2 20 TWIN instrument (Hillsboro, OR, USA) at an acceleration voltage of 200 kV. The SEM/EDX-mapping images were obtained through a SU3500 Scanning Electron Microscope instrument (HITACHI, Tokyo, Japan), wherein the samples were coated with gold prior to observation. The TG/DTG analysis was conducted on a METTLER TOLEDO TGA/DSC2/1600 instrument (Zurich, Switzerland) operating at 50 mL/min N₂ with a heating rate of 10 K/min from 313 to 873 K.

3.2.3. Catalytic Reaction

All the “one-pot” and “one-step” conversion of fructose to DFF were carried in a 5 mL round-bottom flask heated in a temperature-controlled oil bath with magnetic stirring. In a typical catalytic reaction, fructose (45 mg, 0.25 mmol), x -PMo₁₂/PAN or x -PMo₁₂/F_Y-PAN catalyst (30 mg), and DMSO (1 mL) were added into the flask. The mixture was heated to 433 K and incubated at this temperature for 4 h in open air with continuous stirring (400 rpm) under reflux. After the reaction, the reaction mixture was cooled gradually to room temperature. The solid catalyst was then isolated from the mixture by centrifugation. The used catalyst was washed with DMSO (2 mL \times 6) until the filtrate became transparent, dried at 353 K for 10 h, and used for the recycling experiments. The top residual mixture after the centrifugation and the washing DMSO were combined and ready to be analyzed. For the aerobic oxidation of HMF to DFF, 35 mg HMF (35 mg, 0.28 mmol) was used as the substrate while keeping other reaction conditions unchanged (30 mg catalyst, 1 mL DMSO, 433 K, 4 h, in air).

3.2.4. Product Analysis

The quantitative analysis of HMF and DFF was performed on GC (FILI, GC-9790) with an Innowax capillary column (30 m \times 0.25 mm), a hydrogen flame-ionization detector (FID), and a ZB-2020 integrator. The temperature of the injector and detector on GC was 543 K, and benzyl alcohol was used as the internal standard substance. The quantification of FA, LA, FF, etc. was done with an external standard method performing on HPLC (Waters, e2695) with a Bio-Rad Aminex HPX-87 column, a parallax detector, and an ultraviolet detector. The temperatures of the parallax detector and column were 308 and 323 K, respectively. H₂SO₄ (5 mM) was applied as a mobile phase with a flow rate of 0.6 mL/min. The conversion and yields are as defined as follows:

Conversion of substrate (mol%) = (mol of starting substrate - mol of residual substrate) / (mol of starting substrate) \times 100%

Yield of HMF = (mol of HMF produced) / (mol of starting fructose) \times 100%

Yield of DFF = (mol of DFF produced) / (mol of starting substrate) \times 100%

Yield of FA = (mol of FA produced) / (mol of starting substrate) \times 100%

$$\text{Yield of LA} = (\text{mol of LA produced})/(\text{mol of starting substrate}) \times 100\%$$

4. Conclusions

In summary, we report the preparation of bifunctional inorganic–organic hybrid catalysts by supporting keggin-type PMo_{12} HPA on PAN or F-PAN for the “one-pot” and “one-step” synthesis of DFF from fructose. We show that the PMo_{12} HPA is anchored and well-dispersed on the polymer support via site-to-site acid–base interaction between the protons in HPA and the quinoid diimine in PAN, which decreases the Brønsted acidity of the hybrid catalyst while retaining the redox sites of PMo_{12} HPA. The x - PMo_{12} /PAN catalysts ($x = 10\sim 50$) are active for both HMF-to-DFF oxidation and “one-pot” fructose-to-DFF conversion, however, less stable. Notably, we demonstrate that the grafting of the “support” PAN with formyl groups strengthens the dehydration performance of the 40- PMo_{12} /F-PAN catalyst, thereby avoiding the negative influence of water and promoting the tandem fructose-to-DFF transformation. The F-PAN acts as a “support” for anchoring and dispersing PMo_{12} species as well as a co-catalyst for reinforcing the dehydration performance of the PMo_{12} /F-PAN catalyst. A highest DFF yield of 76.7% has been obtained by conducting the “one-pot” and “one-step” conversion over the 40- PMo_{12} /F₃-PAN catalyst at 433 K for 7 h in air. The alleviation of side-product generations and shortened reaction time lower the production energy for fructose-to-DFF conversion. In addition, the 40- PMo_{12} /F₃-PAN catalyst shows good reusability for the fructose-to-DFF conversion, which highlights the designing of novel and stable hybrid inorganic-organic hybrid catalysts for producing important platform furan chemicals from biomass-derived hexose.

Supplementary Materials: The following are available online at <http://www.mdpi.com/2073-4344/9/5/445/s1>, Figure S1: (a) FTIR spectrum and (b) XRD pattern of Keggin-type PMo_{12} HPA, Figure S2: TEM images of (a) PAN, and (b) 40- PMo_{12} /PAN, Figure S3: FTIR spectra of 40- PMo_{12} /PAN catalysts after reacting with different substances, Figure S4: TEM images of (a) F₃-PAN, and (b) 40- PMo_{12} /F₃-PAN, Figure S5: TG and DTG profiles of (a) fresh and (b) spent 40- PMo_{12} /F₃-PAN catalysts, Scheme S1: Schematic illustration of the grafting of formyl groups on PAN support, Table S1: Preparation conditions of F_y-PAN “supports” and the results resolved from the FTIR spectra of F_y-PAN and 40- PMo_{12} /F_y-PAN, Table S2: Comparison of the production rates of several hybrid catalysts in the “one-pot” and “one-step” conversion of fructose to DFF, Table S3: The leaching of PMo_{12} HPA during the recycled use of 40- PMo_{12} /F₃-PAN, Table S4: Recycled use of 40- PMo_{12} /F₃-PAN catalyst in the “one-pot” and “one-step” conversion of fructose to DFF.

Author Contributions: Conceptualization, L.Z. and C.H.; methodology, S.L., J.D. and Z.L.; formal analysis, X.F.; investigation, S.L.; resources, L.Z. and C.H.; data curation, S.L.; writing- original draft preparation, S.L.; writing-review and editing, L.Z. and C.H.; supervision, L.Z. and C.H.; funding acquisition, L.Z. and C.H.

Funding: This research was funded by the Natural Science Foundation of China (No. 21875149), 111 Project (B17030) and the Basal Research Fund of the Central University (2016SCU04B06).

Acknowledgments: We thank Shaolan Wang, Xiaohong Zhu, and Yong Luo in the analytical and testing center of Sichuan University for the TGA, FTIR, and TEM experiments.

Conflicts of Interest: The authors declare no conflict of interest.

References

1. Tuck, C.O.; Perez, E.; Horvath, I.T.; Sheldon, R.A.; Poliakov, M. Valorization of Biomass: Deriving More Value from Waste. *Science* **2012**, *337*, 695–699. [[CrossRef](#)]
2. Liu, B.; Zhang, Z. Catalytic Conversion of Biomass into Chemicals and Fuels over Magnetic Catalysts. *ACS Catal.* **2016**, *6*, 326–338. [[CrossRef](#)]
3. Arevalo-Gallegos, A.; Ahmad, Z.; Asgher, M.; Parra-Saldivar, R.; Iqbal, H.M.N. Lignocellulose: A sustainable material to produce value-added products with a zero waste approach-A review. *Int. J. Biol. Macromol.* **2017**, *99*, 308–318. [[CrossRef](#)]
4. Lynd, L.R.; Liang, X.; Bidy, M.J.; Allee, A.; Cai, H.; Foust, T.; Himmel, M.E.; Laser, M.S.; Wang, M.; Wyman, C.E. Cellulosic ethanol: status and innovation. *Curr. Opin. Biotechnol.* **2017**, *45*, 202–211. [[CrossRef](#)] [[PubMed](#)]
5. Bender, T.A.; Dabrowski, J.A.; Gagne, M.R. Homogeneous catalysis for the production of low-volume, high-value chemicals from biomass. *Nat. Rev. Chem.* **2018**, *2*, 35–46. [[CrossRef](#)]

6. Hu, L.; Lin, L.; Wu, Z.; Zhou, S.; Liu, S. Recent advances in catalytic transformation of biomass-derived 5-hydroxymethylfurfural into the innovative fuels and chemicals. *Renew. Sustain. Energy Rev.* **2017**, *74*, 230–257. [[CrossRef](#)]
7. Kong, X.; Zhu, Y.; Fang, Z.; Kozinski, J.A.; Butler, I.S.; Xu, L.; Song, H.; Wei, X. Catalytic conversion of 5-hydroxymethylfurfural to some value-added derivatives. *Green Chem.* **2018**, *20*, 3657–3682. [[CrossRef](#)]
8. Yadav, G.D.; Sharma, R.V. Biomass derived chemicals: Environmentally benign process for oxidation of 5-hydroxymethylfurfural to 2,5-diformylfuran by using nano-fibrous Ag-OMS-2-catalyst. *Appl. Catal. B-Environ.* **2014**, *147*, 293–301. [[CrossRef](#)]
9. Jia, X.; Ma, J.; Wang, M.; Du, Z.; Lu, F.; Wang, F.; Xu, J. Promoted role of $\text{Cu}(\text{NO}_3)_2$ on aerobic oxidation of 5-hydroxymethylfurfural to 2,5-diformylfuran over VOSO_4 . *Appl. Catal. A-Gen.* **2014**, *482*, 231–236. [[CrossRef](#)]
10. Nie, J.; Liu, H. Efficient aerobic oxidation of 5-hydroxymethylfurfural to 2,5-diformylfuran on manganese oxide catalysts. *J. Catal.* **2014**, *316*, 57–66. [[CrossRef](#)]
11. Chen, J.; Zhong, J.; Guo, Y.; Chen, L. Ruthenium complex immobilized on poly(4-vinylpyridine)-functionalized carbon-nanotube for selective aerobic oxidation of 5-hydroxymethylfurfural to 2,5-diformylfuran. *RSC Adv.* **2015**, *5*, 5933–5940. [[CrossRef](#)]
12. Fang, R.; Luque, R.; Li, Y. Selective aerobic oxidation of biomass-derived HMF to 2,5-diformylfuran using a MOF-derived magnetic hollow Fe-Co nanocatalyst. *Green Chem.* **2016**, *18*, 3152–3157. [[CrossRef](#)]
13. Chatterjee, M.; Ishizaka, T.; Chatterjee, A.; Kawanami, H. Dehydrogenation of 5-hydroxymethylfurfural to diformylfuran in compressed carbon dioxide: an oxidant free approach. *Green Chem.* **2017**, *19*, 1315–1326. [[CrossRef](#)]
14. Yan, Y.; Li, K.; Zhao, J.; Cai, W.; Yang, Y.; Lee, J.-M. Nanobelt-arrayed vanadium oxide hierarchical microspheres as catalysts for selective oxidation of 5-hydroxymethylfurfural toward 2,5-diformylfuran. *Appl. Catal. B-Environ.* **2017**, *207*, 358–365. [[CrossRef](#)]
15. Yan, S.; Li, Y.; Li, P.; Jia, T.; Wang, S.; Wang, X. Fabrication of mesoporous POMs/SiO₂ nanofibers through electrospinning for oxidative conversion of biomass by H₂O₂ and oxygen. *RSC Adv.* **2018**, *8*, 3499–3511. [[CrossRef](#)]
16. Ren, Y.; Yuan, Z.; Lv, K.; Sun, J.; Zhang, Z.; Chi, Q. Selective and metal-free oxidation of biomass-derived 5-hydroxymethylfurfural to 2,5-diformylfuran over nitrogen-doped carbon materials. *Green Chem.* **2018**, *20*, 4946–4956. [[CrossRef](#)]
17. Yuan, Z.; Liu, B.; Zhou, P.; Zhang, Z.; Chi, Q. Aerobic oxidation of biomass-derived 5-hydroxymethylfurfural to 2,5-diformylfuran with cesium-doped manganese dioxide. *Catal. Sci. Technol.* **2018**, *8*, 4430–4439. [[CrossRef](#)]
18. Zhao, J.; Chen, X.; Du, Y.; Yang, Y.; Lee, J.-M. Vanadium-embedded mesoporous carbon microspheres as effective catalysts for selective aerobic oxidation of 5-hydroxymethyl-2-furfural into 2, 5-diformylfuran. *Appl. Catal. A-Gen.* **2018**, *568*, 16–22. [[CrossRef](#)]
19. Zhang, Z.; Yuan, Z.; Tang, D.; Ren, Y.; Lv, K.; Liu, B. Iron Oxide Encapsulated by Ruthenium Hydroxyapatite as Heterogeneous Catalyst for the Synthesis of 2,5-Diformylfuran. *ChemSusChem* **2014**, *7*, 3496–3504. [[CrossRef](#)]
20. Xu, F.; Zhang, Z. Polyaniline-Grafted VO(acac)₂: An Effective Catalyst for the Synthesis of 2,5-Diformylfuran from 5-Hydroxymethylfurfural and Fructose. *ChemCatChem* **2015**, *7*, 1470–1477. [[CrossRef](#)]
21. Hou, W.; Wang, Q.; Guo, Z.; Li, J.; Zhou, Y.; Wang, J. Nanobelt alpha-CuV₂O₆ with hydrophilic mesoporous poly(ionic liquid): a binary catalyst for synthesis of 2,5-diformylfuran from fructose. *Catal. Sci. Technol.* **2017**, *7*, 1006–1016. [[CrossRef](#)]
22. Liu, Y.; Zhu, L.; Tang, J.; Liu, M.; Cheng, R.; Hu, C. One-pot, One-step Synthesis of 2,5-Diformylfuran from Carbohydrates over Mo-Containing Keggin Heteropolyacids. *ChemSusChem* **2014**, *7*, 3541–3547. [[CrossRef](#)] [[PubMed](#)]
23. Liu, R.; Chen, J.; Chen, L.; Guo, Y.; Zhong, J. One-Step Approach to 2,5-Diformylfuran from Fructose by Using a Bifunctional and Recyclable Acidic Polyoxometalate Catalyst. *ChemPlusChem* **2014**, *79*, 1448–1454. [[CrossRef](#)]
24. Lv, G.; Wang, H.; Yang, Y.; Deng, T.; Chen, C.; Zhu, Y.; Hou, X. Direct synthesis of 2,5-diformylfuran from fructose with graphene oxide as a bifunctional and metal-free catalyst. *Green Chem.* **2016**, *18*, 2302–2307. [[CrossRef](#)]

25. Rathod, P.V.; Nale, S.D.; Jadhav, V.H. Metal Free Acid Base Catalyst in the Selective Synthesis of 2,5-Diformylfuran from Hydroxymethylfurfural, Fructose, and Glucose. *ACS Sustain. Chem. Eng.* **2017**, *5*, 701–707. [[CrossRef](#)]
26. Yang, Z.; Qi, W.; Su, R.; He, Z. 3D Flower-like Micro/Nano Ce-Mo Composite Oxides as Effective Bifunctional Catalysts for One-Pot Conversion of Fructose to 2,5-Diformylfuran. *ACS Sustain. Chem. Eng.* **2017**, *5*, 4179–4187. [[CrossRef](#)]
27. Zhao, J.; Jayakumar, A.; Hu, Z.-T.; Yan, Y.; Yang, Y.; Lee, J.-M. MoO₃-Containing Protonated Nitrogen Doped Carbon as a Bifunctional Catalyst for One-Step Synthesis of 2,5-Diformylfuran from Fructose. *ACS Sustain. Chem. Eng.* **2018**, *6*, 284–291. [[CrossRef](#)]
28. Zhao, J.; Jayakumar, A.; Lee, J.-M. Bifunctional Sulfonated MoO₃-ZrO₂ Binary Oxide Catalysts for the One-Step Synthesis of 2,5-Diformylfuran from Fructose. *ACS Sustain. Chem. Eng.* **2018**, *6*, 2976–2982. [[CrossRef](#)]
29. Zhang, W.; Meng, T.; Tang, J.; Zhuang, W.; Zhou, Y.; Wang, J. Direct Synthesis of 2,5-Diformylfuran from Carbohydrates Using High-Silica MOR Zeolite-Supported Isolated Vanadium Species. *ACS Sustain. Chem. Eng.* **2017**, *5*, 10029–10037. [[CrossRef](#)]
30. Chen, J.; Guo, Y.; Chen, J.; Song, L.; Chen, L. One-Step Approach to 2,5-Diformylfuran from Fructose by Proton-and Vanadium-Containing Graphitic Carbon Nitride. *ChemCatChem* **2014**, *6*, 3174–3181. [[CrossRef](#)]
31. Fang, R.; Luque, R.; Li, Y. Efficient one-pot fructose to DFF conversion using sulfonated magnetically separable MOF-derived Fe₃O₄ (111) catalysts. *Green Chem.* **2017**, *19*, 647–655. [[CrossRef](#)]
32. Mittal, N.; Nisola, G.M.; Malihan, L.B.; Seo, J.G.; Kim, H.; Lee, S.-P.; Chung, W.-J. One-pot synthesis of 2,5-diformylfuran from fructose using a magnetic bi-functional catalyst. *RSC Adv.* **2016**, *6*, 25678–25688. [[CrossRef](#)]
33. Sarmah, B.; Satpati, B.; Srivastava, R. One-pot tandem conversion of monosaccharides and disaccharides to 2,5-diformylfuran using a Ru nanoparticle-supported H-beta catalyst. *Catal. Sci. Technol.* **2018**, *8*, 2870–2882. [[CrossRef](#)]
34. Ma, B.; Wang, Y.; Guo, X.; Tong, X.; Liu, C.; Wang, Y.; Guo, X. Photocatalytic synthesis of 2,5-diformylfuran from 5-hydroxymethylfurfural or fructose over bimetallic Au-Ru nanoparticles supported on reduced graphene oxides. *Appl. Catal. A-Gen.* **2018**, *552*, 70–76. [[CrossRef](#)]
35. Raut, A.B.; Bhanage, B.M. Co-Al Hydrotalcites: Highly Active Catalysts for the One-Pot Conversion of Fructose to 2,5-Diformylfuran. *Chemistryselect* **2018**, *3*, 11388–11397. [[CrossRef](#)]
36. Wang, Z.M.; Liu, L.-J.L.; Xiang, B.; Wang, Y.; Lyu, Y.J.; Qi, T.; Si, Z.B.; Yang, H.Q.; Hu, C.W. The design and catalytic performance of molybdenum active sites on an MCM-41 framework for the aerobic oxidation of 5-hydroxymethylfurfural to 2,5-diformylfuran. *Catal. Sci. Technol.* **2019**, *9*, 811–821. [[CrossRef](#)]
37. Gu, B.; He, S.; Zhou, W.; Kang, J.; Cheng, K.; Zhang, Q.; Wang, Y. Polyaniline-supported iron catalyst for selective synthesis of lower olefins from syngas. *J. Energy Chem.* **2017**, *26*, 608–615. [[CrossRef](#)]
38. Patel, H.A.; Sawant, A.M.; Rao, V.J.; Patel, A.L.; Bedekar, A.V. Polyaniline Supported FeCl₃: An Effective Heterogeneous Catalyst for Biginelli Reaction. *Catal. Lett.* **2017**, *147*, 2306–2312. [[CrossRef](#)]
39. Samai, B.; Bhattacharya, S.C. Conducting polymer supported cerium oxide nanoparticle: Enhanced photocatalytic activity for waste water treatment. *Mater. Chem. Phys.* **2018**, *220*, 171–181. [[CrossRef](#)]
40. Jesus Garcia-Fernandez, M.; Mercedes Pastor-Blas, M.; Epron, F.; Sepulveda-Escribano, A. Proposed mechanisms for the removal of nitrate from water by platinum catalysts supported on polyaniline and polypyrrole. *Appl. Catal. B-Environ.* **2018**, *225*, 162–171. [[CrossRef](#)]
41. Das, S.; Dutta, K.; Kundu, P.P.; Bhattacharya, S.K. Nanostructured Polyaniline: An Efficient Support Matrix for Platinum-Ruthenium Anode Catalyst in Direct Methanol Fuel Cell. *Fuel Cells* **2018**, *18*, 369–378. [[CrossRef](#)]
42. Liu, Y.; Tang, D.; Cao, K.; Yu, L.; Han, J.; Xu, Q. Probing the support effect at the molecular level in the polyaniline-supported palladium nanoparticle-catalyzed Ullmann reaction of aryl iodides. *J. Catal.* **2018**, *360*, 250–260. [[CrossRef](#)]
43. Tanwar, R.; Kaur, B.; Mandal, U.K. Highly efficient and visible light driven Ni_{0.5}Zn_{0.5}Fe₂O₄@PANI modified BiOCl heterocomposite catalyst for water remediation. *Appl. Catal. B-Environ.* **2017**, *211*, 305–322. [[CrossRef](#)]
44. Gallon, B.J.; Kojima, R.W.; Kaner, R.B.; Diaconescu, P.L. Palladium nanoparticles supported on polyaniline nanofibers as a semi-heterogeneous catalyst in water. *Angew. Chem. Int. Ed.* **2007**, *46*, 7251–7254. [[CrossRef](#)]
45. Zhu, L.; Dai, J.; Liu, M.; Tang, D.; Liu, S.; Hu, C. Formyl-Modified Polyaniline for the Catalytic Dehydration of Fructose to 5-Hydroxymethylfurfural. *ChemSusChem* **2016**, *9*, 2174–2181. [[CrossRef](#)]

46. Dai, J.; Zhu, L.; Tang, D.; Fu, X.; Tang, J.; Guo, X.; Hu, C. Sulfonated polyaniline as a solid organocatalyst for dehydration of fructose into 5-hydroxymethylfurfural. *Green Chem.* **2017**, *19*, 1932–1939. [[CrossRef](#)]
47. Dai, J.; Liu, Z.; Hu, Y.; Liu, S.; Chen, L.; Qi, T.; Yang, H.; Zhu, L.; Hu, C. Adjusting the acidity of sulfonated organocatalyst for the one-pot production of 5-ethoxymethylfurfural from fructose. *Catal. Sci. Technol.* **2019**, *9*, 483–492. [[CrossRef](#)]
48. Tsigdinos, G.A.; Hallada, C.J. Molybdovanadophosphoric Acids and Their Salts. I. Investigation of Methods of Preparation and Characterization. *Inorg. Chem.* **1968**, *7*, 437–441. [[CrossRef](#)]
49. Nandi, M.; Gangopadhyay, R.; Bhaumik, A. Mesoporous polyaniline having high conductivity at room temperature. *Microporous Mesoporous Mater.* **2008**, *109*, 239–247. [[CrossRef](#)]
50. Thiemann, C.; Brett, C.M.A. Electropolymerisation and properties of conducting polymers derived from aminobenzenesulphonic acids and from mixtures with aniline. *Synth. Met.* **2001**, *125*, 445–451. [[CrossRef](#)]
51. Cao, Y.; Li, S.Z.; Xue, Z.J.; Guo, D. Spectroscopic and electrical characterization of some aniline oligomers and polyaniline. *Synth. Met.* **1986**, *16*, 305–315. [[CrossRef](#)]
52. Kang, E.T.; Neoh, K.G.; Tan, K.L. Polyaniline: A polymer with many interesting intrinsic redox states. *Prog. Polym. Sci.* **1998**, *23*, 277–324. [[CrossRef](#)]
53. Trchova, M.; Sedenkova, I.; Konyushenko, E.N.; Stejskal, J.; Holler, P.; Ciric-Marjanovic, G. Evolution of polyaniline nanotubes: The oxidation of aniline in water. *J. Phys. Chem. B* **2006**, *110*, 9461–9468. [[CrossRef](#)] [[PubMed](#)]
54. Furukawa, Y.; Ueda, F.; Hyodo, Y.; Harada, I.; Nakajima, T.; Kawagoe, T. Vibrational-spectra and structure of polyaniline. *Macromolecules* **1988**, *21*, 1297–1305. [[CrossRef](#)]
55. Xing, S.X.; Zheng, H.W.; Zhao, G.K. Preparation of polyaniline nanofibers via a novel interfacial polymerization method. *Synth. Met.* **2008**, *158*, 59–63. [[CrossRef](#)]
56. Pouget, J.P.; Jozefowicz, M.E.; Epstein, A.J.; Tang, X.; Macdiarmid, A.G. X-ray structure of polyaniline. *Macromolecules* **1991**, *24*, 779–789. [[CrossRef](#)]
57. Gong, J.; Hua, R.N.; Xie, Z.W.; Wang, S.G.; Qu, L.Y. Chemical syntheses of the conducting material formed by heteropolyacids and polyaniline. *Polym. J.* **2001**, *33*, 377–382. [[CrossRef](#)]
58. Xing, S.X.; Zhao, C.; Jing, S.Y.; Wang, Z. Morphology and conductivity of polyaniline nanofibers prepared by ‘seeding’ polymerization. *Polymer* **2006**, *47*, 2305–2313. [[CrossRef](#)]
59. Liao, Y.; Strong, V.; Chian, W.; Wang, X.; Li, X.-G.; Kaner, R.B. Sulfonated Polyaniline Nanostructures Synthesized via Rapid Initiated Copolymerization with Controllable Morphology, Size, and Electrical Properties. *Macromolecules* **2012**, *45*, 1570–1579. [[CrossRef](#)]
60. Papagianni, G.G.; Stergiou, D.V.; Armatas, G.S.; Kanatzidis, M.G.; Prodromidis, M.I. Synthesis, characterization and performance of polyaniline-polyoxometalates (XM₁₂, X = P, Si and M = Mo, W) composites as electrocatalysts of bromates. *Sens. Actuators B* **2012**, *173*, 346–353. [[CrossRef](#)]
61. Cui, J.; Tan, J.; Deng, T.; Cui, X.; Zhu, Y.; Li, Y. Conversion of carbohydrates to furfural via selective cleavage of the carbon–carbon bond: the cooperative effects of zeolite and solvent. *Green Chem.* **2016**, *18*, 1619–1624. [[CrossRef](#)]
62. Wang, Y.Q.; Yang, X.H.; Zheng, H.Y.; Li, X.Q.; Zhu, Y.L.; Li, Y.W. Mechanistic insights on catalytic conversion fructose to furfural on beta zeolite via selective carbon-carbon bond cleavage. *Mol. Catal.* **2019**, *463*, 130–139. [[CrossRef](#)]

